4 Local-to-Bulk Electronic Correlation Project

– Emerging phenomena induced by deformation of local structure in strongly correlated electron system –

Project Leader: Masaki Fujita

4-1 Background and purpose of the project

Since the discovery of superconductivity in lamellar cuprate oxides, their physical properties have been intensively studied in connection with the occupation of oxygen atoms. The superconducting transition temperature (T_c) in $YBa_2Cu_3O_{6+\delta}$ can be controlled by the number of oxygen atoms in the unit cell. More recently, the relationship between the ground states and the local structure of oxygen atoms near the CuO_2 plane has attracted much interest. $RE_{2-x}Ce_xCuO_4$ (RE = rare esarth element) with a Nd_2CuO_4-type (T'-type) structure in which Cu ions have fourfold coplanar coordination is a typical electron-doped cuprate superconductor (Fig.1(a)). An as-sintered (AS) sample of T'-type $RE_{2-x}Ce_xCuO_4$ is insulators up to the heavy Ce concentration region, and superconductivity emerges after an adequate oxygen reduction annealing procedure. Even more importantly, superconducting transition (undoped superconductivity) has been reported for thin films and low-temperature synthesized powder samples of Ce-free T'-type RE_2CuO_4 [1, 2], which has been recognized as an antiferromagnetic (AF) Mott insulator for a long time. Furthermore, recent theoretical studies considering the local structure around the CuO_2 plane clarified that the parent compounds of T'-type RE_2CuO_4 can have a metallic nature, in contrast to the insulating nature of La_2CuO_4 with a K_2NiF_4-type (T-type) structure [3, 4]. Therefore, the determination of the genuine ground state in T'-RE_2CuO_{4-y} and the relation with local structure, namely, oxygen ordination around Cu, is now an essential issue in the research of high-T_c superconductivity. In this project, we investigated the electronic state of the RE_2CuO_4 family with quantum beams such as neutrons, synchrotron X-rays, and muons to clarify the common mechanism of the superconducting transition in cuprate oxide.

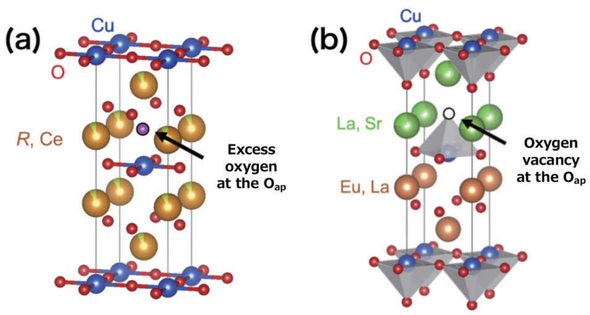

Fig. 1: Crystal structure of $R_2CuO_{4+\delta}$. (R: rare earth) with (a) T'- and (b) T^*-type cuprates. T'(T^*)-type cuprate has flat CuO_2 planes (CuO_5 pyramid) with four (five) coordination for Cu ions. In the AS T'(T^*)-type cuprate, excess oxygen (oxygen vacancy) is considered to exist at an apical oxygen site.

4-2 Annealing effect on the electronic state in *T'*-type cuprate [5, 6, 7]

It has been reported that low-temperature synthesized T'-type $La_{1.8}Eu_{0.2}CuO_4$ (LECO) exhibits superconductivity with T_c ~ 25 K [2]. Because a powder sample of LECO can be available, the magnetic properties were investigated by muon spin rotation/relaxation (μSR) and nuclear magnetic resonance measurements [8, 9]. However, the variation in the electronic state due to annealing associated with the appearance of superconductivity is still unclear. Therefore, we performed Cu K-edge X-ray absorption near-edge structure (XANES) measurements on LECO as well as the high-temperature synthesized Nd_2CuO_4 (NCO) and Pr_2CuO_4 (PCO). NCO and PCO do not show

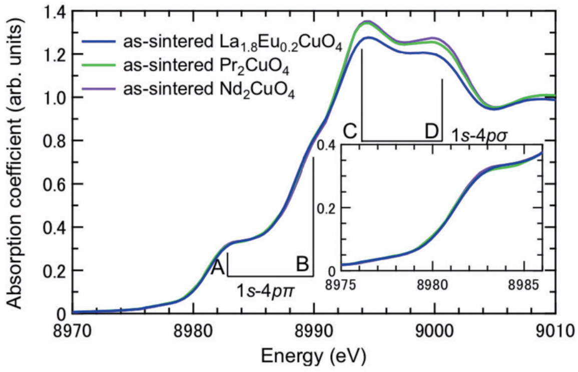

Fig. 2: XANES spectra for as-sintered powder samples of $La_{1.8}Eu_{0.2}CuO_4$, Nd_2CuO_4 and Pr_2CuO_4. The inset is the enlarged spectra in the range from 8975 eV to 8986 eV.

superconductivity even after annealing. Therefore, information on the undoped superconductivity could be obtained by comparing the annealing effects of the electronic states of these samples. First, we show the XANES spectra of the AS samples in Fig. 2. All spectra have quite similar structures, indicating the same electronic state in the AS samples, regardless of the synthesis method. The small difference at ~8994 eV and ~9000 eV corresponds to 1s-4p_σ transitions and is attributed to the size of rare-earth elements [10]. Because the optical conductivity spectra of AS NCO have a clear gap structure, the similarity in the XANES spectra suggests the Mott insulating nature of AS LECO.

Next, we show the spectra of the annealed (AN) samples. In Fig. 2, the red lines represent the XANES spectra for the AN samples. The variation in the spectra due to annealing is significant for LECO, while the annealing effect on the spectra of NCO and PCO is small. This observation first demonstrated the different annealing effects on the electronic state between the system with and without superconductivity. For a clear visualization of the annealing effect on the spectra, the difference spectra are shown in the lower column. The results were obtained by subtracting the spectra for the AS sample from that for the AN sample. Note that the peak at ~8981 eV corresponds to the 1s-4$p\pi$ Cu^+ transition. Thus, the appearance of intensity indicates the production of Cu^+, that is, electron doping into the Cu site due to annealing, as is a similar case for Ce-substitution. The electrons are induced in NCO and PCO due to annealing, but the intensity is much weaker than that for LECO. Combined with the previous results for as-sintered $Pr_{2-x}Ce_xCuO_4$, we evaluated the density of induced electrons per Cu (n_{AN}) to be 0.40 for ECO and 0.05 for NCO and PCO, respectively. On the other hand, the amount of oxygen loss due to annealing (δ~0.035-0.05) is comparable. Therefore, the increases in electron density for LECO and the other two samples occur in different processes. As for NCO and PCO, n_{AN} and δ approximately follow the $n_{AN} = 2\delta$ relation, which is derived from the picture that electrons are doped into the Cu 3$d_{x^2-y^2}$ upper Hubbard band (UHB). However, the emergence of electrons more than 2δ is difficult to understand within this picture and suggests the generation of holes, which compensate for electrons to hold charge

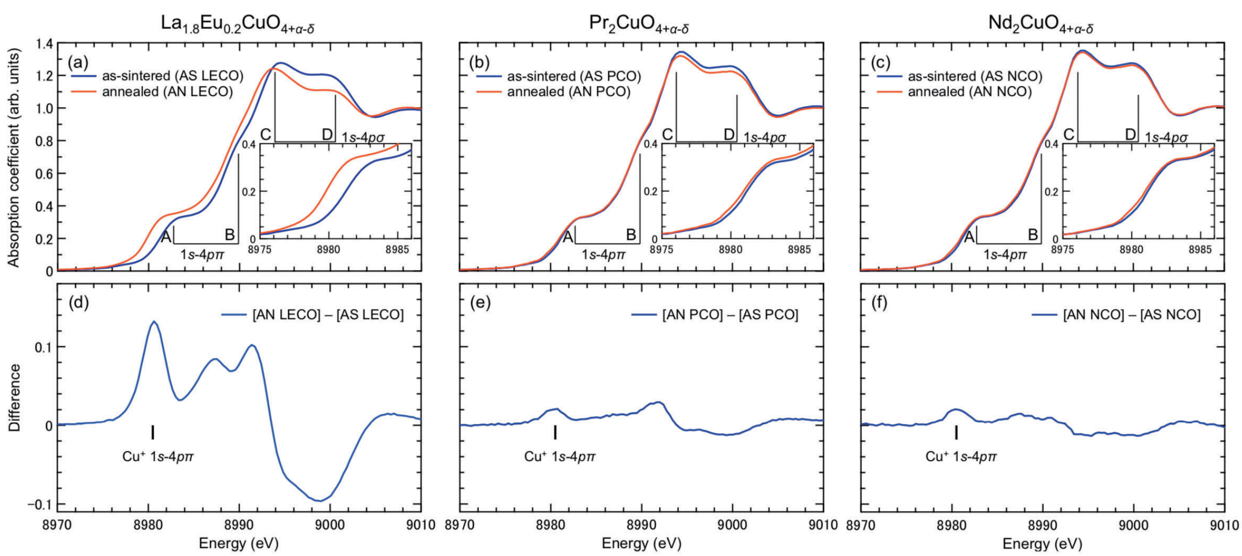

Fig. 3: (a) XANES spectra for as-sintered and annealed (a) $La_{1.8}La_{0.2}CuO_4$, (b) Pr_2CuO_4 and (c) Nd_2CuO_4. Differential spectra between annealed and as-sintered (d) $La_{1.8}La_{0.2}CuO_4$, (e) Pr_2CuO_4 and (f) Nd_2CuO_4.

neutrality. For the simultaneous emergence of electrons and holes, the charge transfer (CT) gap should collapse so that the Fermi level is located in the hybridized UHB and O 2*p* bands. Such a situation would be caused by the removal of apical oxygen, which potentially lowers the Madelung energy of the UHB [11] to touch with the O 2*p* band. Because the energy of the CT gap is negatively proportional to the in-plane Cu-O bond length, the CT gap in LECO, which has the largest in-plane lattice constant, is expected to be small in *T*'-type RE_2CuO_4. As a result, the effect of oxygen reduction on the electronic state is sensitive in LECO compared to NCO and PCO.

4-3 Magnetic and superconducting properties in *T**-type cuprate [12, 13, 14]

Other reference systems are required for further studies on the relationship between Cu coordination and the ground state. A single-layer *T**-type cuprate with CuO_5 pyramid coordination is a candidate system. The crystal structure of *T**-type cuprate is composed of rock-salt layers in the *T*-type cuprate, and by fluorite layers in the *T*'-type cuprate with alternating stacking along the c direction (See Fig. 1(b)).

Akimitsu and coworkers successfully synthesized superconducting *T**-type $Nd_{2-x-y}Ce_xSr_yCuO_4$ with hole doping (T_c ~ 32 K) [15]. For the emergence of superconductivity in *T**-type cuprates, oxidation annealing under high pressures is necessary. The role of annealing is considered to repair the oxygen defects at the apical oxygen site, which partially exists in the AS compound. The repair of oxygen defects is in contrast to the removal of excess oxygen to induce superconductivity in *T*'-type cuprates [16]. Thus, *T**-type

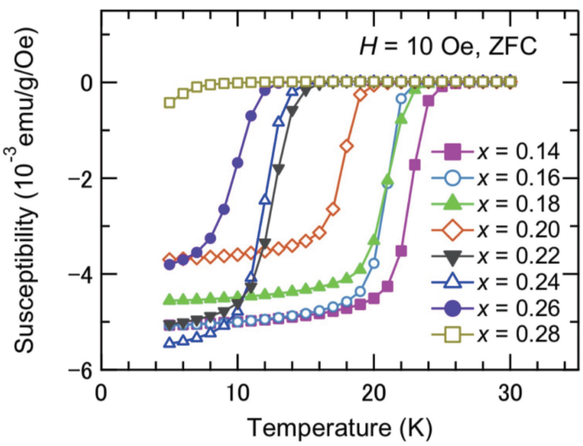

Fig. 4: Temperature dependence of magnetic susceptibility measured after zero-field-cooling process for the oxidation annealed *T**-$La_{1-x/2}Eu_{1-x/2}SrxCuO_4$.

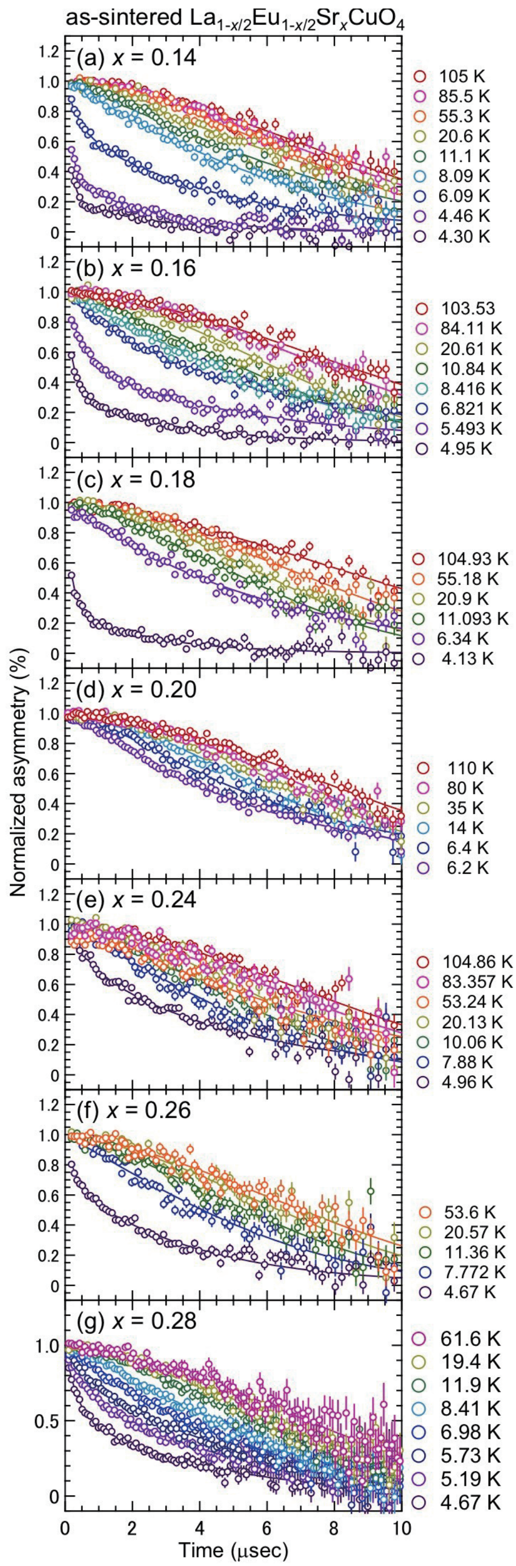

Fig. 5: Zero-field μSR time spectra for the as-sintered *T**-$La_{1-x/2}Eu_{1-x/2}Sr_xCuO_4$. Spectra are normalized after subtraction of constant background.

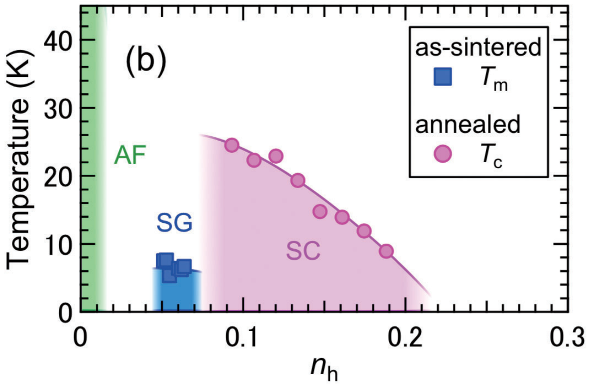

Fig. 6: Magnetic (T_m) and superconducting (SC) transition temperatures (T_c) in as-sintered and oxidation annealed $La_{1-x/2}Eu_{1-x/2}Sr_xCuO_4$ as a function of the hole density (n_h). Green, blue, and pink areas represent the antiferromagnetic ordered (AF), spin-glass (SG), and SC states, respectively. Solid lines are guides to the eyes.

cuprates are suitable references for studying the relationship between the local crystal structure, Cu coordination, and the ground state.

We synthesized T^*-structured $La_{1-x/2}Eu_{1-x/2}Sr_xCuO_4$ (LESCO) with $0.12 \leq x \leq 0.28$ and performed the first μSR, magnetic susceptibility, and electric resistivity measurements of both AS and oxidation annealed (OA) samples. As shown in Fig. 4, all AS samples exhibit evidence of superconducting transition, although the transition temperature is low, and the Meissner signal is weak at $x = 0.28$. T_c (onset) decreases with increasing Sr concentration. Meanwhile, the development of spin correlations can be seen in the zero-field μSR time spectra for the AS samples. That is, a Gaussian-type time spectrum at high temperatures transforms into an exponential one upon cooling (Fig. 5). From the qualitative analysis of the temperature dependence of μSR time spectra, we determined the onset temperature for the appearance of the fast depolarization component in the μSR time spectra (T_m) to be ~6-8 K for all AS samples. Thus, the ground state of LESCO at a broad Sr concentration is drastically varied due to oxidation annealing.

To estimate the actual hole density (n_h) and to draw a phase diagram of T^*-type LESCO, we carried out O *K*-edge X-ray absorption spectroscopy measurements. As a result, we found that n_h is smaller than x in the AS samples, and n_h drastically increases due to annealing. (Not shown) Increased n_h cannot be explained only by the oxygen gain due to annealing. These results suggest that the hole introduced by Sr substitution is delocalized outside the CuO_2 plane (a block layer and/or oxygen-deficient site) in the AS samples. Such holes enter the CuO_2 plane due to annealing. In Fig. 6, the phase diagram of LESCO is plotted against n_h. In the figure, the μSR result reporting the appearance of long-range magnetic order below ~170 K in T^*-type parent $La_{1.2}Tb_{0.8}CuO_4$ is referred [17]. The overall phase diagram is similar to that for *T*-type LSCO. However, T_c increases with decreasing n_h at least to 0.09. This behavior is somewhat different from the dome-shaped nh-dependence of T_c with nh for the optimal T_c of 0.16. The increase in T_c in the lightly doped region toward zero doping is similar to the phase diagram of hole-doped T'-type $La_{1.8-x}Eu_{0.2}Ca_xCuO_4$. Thus, the physical properties of the lightly doped and undoped T^*-type cuprates should be clarified by further study to gain a unified understanding of the relationship between the ground state and oxygen ordination around Cu in the RE_2CuO_4 family.

4-4 Project workshop

To exchange information and ideas, we held a three-day workshop during December 20th and 22nd in Ibusuki, Kagoshima prefecture. The group member of this project organized the workshop, and the CMRC partially supported the workshop. The workshop started with the review talk on the recent studies of T'-type cuprate by Prof. Adachi (Sophia Univ.), and an individual talk on their research followed it. We shared exciting results and discussed the prospects of research on superconductivity and quantum beams. The workshop received high marks from the participants.

Fig. 7: A group photo of the workshop held in Hotel Ibusuki during December 20th and 22nd.

References

[1] M. Naito, S Karimoto, and A. Tsukada: Supercond. Sci. Technol. **15** (2002) 1663.

[2] T. Takamatsu, M. Kato, T. Noji, Y. Koike, Applied Physics Express, **5** (2012) 073101.
[3] H. Das and T. Saha-Dasgupta, Phys. Rev. B **79** (2009) 134522.
[4] C. Weber, K. Haule, and G. Kotilar: Nature Phys. **6** (2010) 574.
[5] S Asano, K M Suzuki, D Matsumura, K Ishii, T Ina, and M. Fujita, J. Phys.: Conf. Ser. **969** (2018) 012051.
[6] S. Asano, K. Ishii, D. Matsumura, T. Tsuji, T. Ina, K. M. Suzuki, and M. Fujita, J. Phys. Soc. Jpn. **87** (2018) 094710.
[7] S. Asano, K. Ishii, D. Matsumura, T. Tsuji, K. Kudo, T. Taniguchi, S. Saito, T. Sunohara, T. Kawamata, Y. Koike, and M. Fujita, in preparation.
[8] T. Adachi, A. Takahashi, K. M. Suzuki, M. A. Baqiya, T. Konno, T. Takamatsu, M. Kato, I. Watanabe, A. Koda, M. Miyazaki, R. Kadono, and Y. Koike, J. Phys. Soc. Jpn. **85** (2016) 114716.
[9] H. Fukazawa, S. Ishiyama, M. Goto, S. Kanamaru, K. Ohashi, T. Kawamata, T. Adachi, M. Hirata, T. Sasaki, Y. Koike and Y. Kohori, Physica C, **541** (2017) 30.
[10] G. Liang, Y. Guo, D. Badresingh, W. Xu, Y. Tang, M. Croft, J. Chen, A. Sahiner, B.-h. O, and J. T. Markert, Phys. Rev. B **51** (1995) 1258.
[11] T. Adachi, Y. Mori, A. Takahashi, M. Kato, T. Nishizaki, T. Sasaki, N. Kobayashi, and Y. Koike, J. Phys. Soc. Jpn. **82** (2013) 063713.
[12] M. Fujita, K. M. Suzuki, S. Asano, A. Koda, H. Okabe, and R. Kadono, JPS Conf. Proc. **21** (2018) 011026.
[13] S. Asano, K. M. Suzuki, K. Kudo, I. Watanabe, A. Koda, R. Kadono, T. Noji, Y. Koike, T. Taniguchi, S. Kitagawa, K. Ishida, and M. Fujita, J. Phys. Soc. Jpn. **88** (2019) 084709.
[14] S. Asano, K. Ishii, K. Yamagami, J. Miyawaki, Y. Harada, and M. Fujita, in preparation.
[15] J. Akimitsu, S. Suzuki, M. Watanabe, and H. Sawa, Jpn. J. Appl. Phys. **27** (1988) L1859.
[16] P. G. Radaelli, J. D. Jorgensen, A. J. Schultz, J. L. Peng, and R. L. Greene: Phys. Rev. B **49** (1994) 15322, A. J. Schultz, J. D. Jorgensen, J. L. Peng, and R. L. Greene: Phys. Rev. B **53** (1996) 5157.
[17] A. Lappas, K. Prassides, A. Amato, R. Feyerherm, F. N. Gygax, and A. Schenck, Hyperfine Interact. **86**, (1994) 555.